Available online at www.sciencedirect.com

ScienceDirect

Procedia Engineering 00 (2016) 000–000

Procedia Engineering

www.elsevier.com/locate/procedia

1st International Conference on the Material Point Method, MPM 2017

Slope failure simulations with MPM

Phil J. Vardon[a,*], Bin Wang[a], Michael A. Hicks[a]

[a]*Geo-Engineering Section, Delft University of Technology, Delft, The Netherlands*

Abstract

The simulation of slope failures, including both failure initiation and development, has been modelled using the material point method. By utilising a constitutive model which encompasses, in a simplified manner, both pre- and post-failure behaviour, the majority of types of geotechnical slope failure can be observed in the simulations. This is a step towards being able to better quantify the consequences of slope failures and thereby to a better quantification of risk. Numerical case studies involving various slope angles, heterogeneity and rainfall induced slope failures are presented to demonstrate the ability of the method to simulate commonly observed failure modes.

Peer-review under responsibility of the organizing committee of the 1 st International Conference on the Material Point Method.

Keywords: heterogeneity; material point method; rainfall induced; slope failure; strain softening.

1. Introduction

Slope stability methods typically involve only the initial failure of the slope, although the risk from slope failure also depends on the failure consequence. For example, a superficial slide, or an initial failure which results in a minor crest displacement, may not result in a significant consequence. Conversely, a minor initial slide, which has the effect of triggering a larger slide or series of slides, may have a much greater consequence and therefore risk.

In this work, a version of the material point method (MPM) has been implemented and used to investigate the failure behaviour of slopes. A series of numerical case studies, presented previously across various papers by the authors, have been examined together to illustrate the behaviour and the ability to simulate a number of commonly observed failure modes. In so doing, this illustrates the potential for the material point method to be used in

* Corresponding author.
E-mail address: p.j.vardon@tudelft.nl

Peer-review under responsibility of the organizing committee of the 1 st International Conference on the Material Point Method.

conjunction with risk-based assessment methods more satisfactorily than other methods, such as the finite element method, where only the initial stability is considered. A secondary objective is to summarise the work undertaken by the authors on slope failures with MPM.

Several types of soil slope failure have been observed and categorised [1-4] and these are schematically presented in Fig. 1. They range from single rotational failures (Fig. 1(a)), which can be small or large, to large translational slides (Fig. 1(b)), to superficial slides (Fig. 1(c)), to material or earthflows (Fig. 1(d)). In all cases, the shear strength of the material is exceeded by the shear stress and a movement of material is observed. A variety of underlying driving mechanisms, e.g. rainfall or weathering [5], or changes in geometry, e.g. toe erosion, can trigger the failures, but it is the material behaviour during the failure which governs how the failure progresses or not. In Fig. 1(d), (e) and (f) the changing geometry controls the failure development.

Typical assessment methods for the stability of slopes include the following: (i) the limit equilibrium method (LEM), where a prescribed failure type is given, the geometry of the failure varied (within prescribed bounds), and the lowest ratio between the available resistance and the driving forces given as a Factor of Safety (FoS); (ii) the finite element method (FEM), or other similar numerical method, where the material behaviour and geometry are characterised and the initial stability is assessed, typically by reducing the strength of the material until deformations exceed a limiting value. In the first method, some knowledge of the assessed mechanism is required, although this disadvantage is at least partly offset by advantages in computational speed and conceptual simplicity. However, no insight can be gained in terms of the behaviour during the failure, displacements, or behaviour after the failure, without special treatment. FEM does not prescribe the failure mechanism, but, without special treatment, cannot predict the behaviour once the deformations have exceeded a certain limit, due to mesh tangling, and so FEM analyses often do not include features of post-failure behaviour. The material point method [6] utilises the advantages of FEM to prescribe geometry, boundary conditions and material behaviour, while not prescribing failure type, while also allowing the material to move through the mesh and thereby allowing observation of the ongoing failure and final geometry.

This paper is based on the MPM formulation presented in [7], an initial investigation of slope failures in [8], an investigation into the impact of heterogeneity in [9] and rainfall induced slope failure in [10].

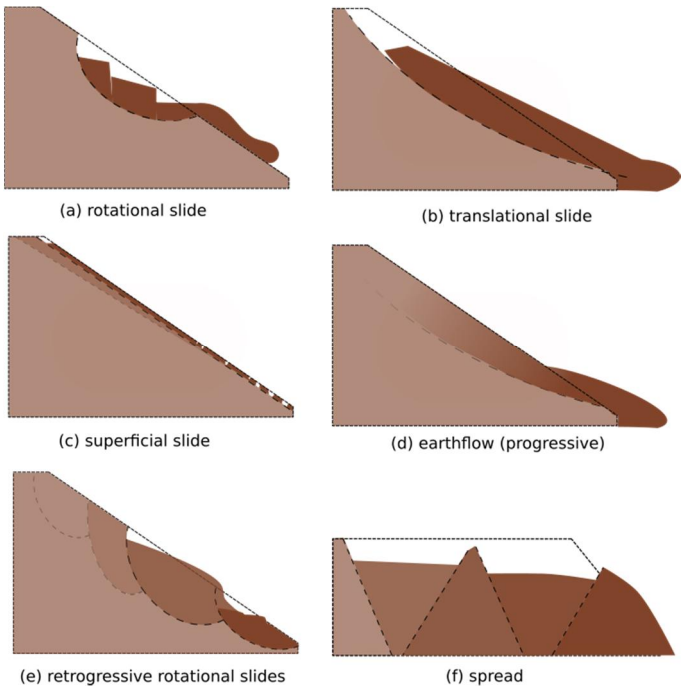

Fig. 1. Geotechnical slope failure types (after [1-4]).

2. Formulation and material model

A version of MPM has been used [7], which has been written in such a way that both quasi-static and dynamic analyses can be undertaken, and implicit and explicit time integration schemes chosen. Where unsaturated conditions prevail, a coupled hydro-mechanical version has been utilised [10], where Bishop's stress is used to give the suction dependent strength change.

The main computational cycle in MPM is illustrated in Fig. 2. Firstly, the state variables, e.g. velocity, acceleration, material stiffness and stress state are mapped onto the nodes of the background mesh (Fig. 2(a)); secondly, a FEM analysis is undertaken, where the mesh is allowed to update its position along with the material points (using Updated Lagrangian FEM) (Fig. 2(b)); and finally, the mesh is reset, with the material points remaining in their updated positions, i.e. they convect through the mesh (Fig. 2(c)).

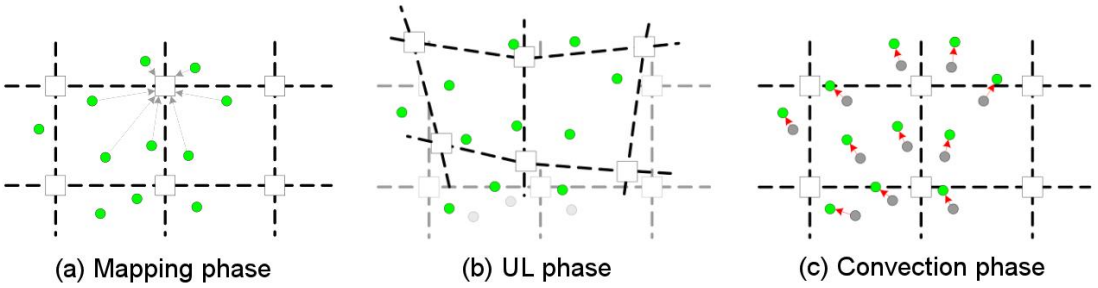

Fig. 2. The main computational phases of MPM [7].

A large strain formulation, accounting for rate independent conditions and rotations, is used. Local damping is added by using a simple damping force with a magnitude proportional to the out of balance forces, and a friction boundary condition has been implemented such that the sliding resistance is controlled by the magnitude of the normal stresses [7]. Two constitutive models have been implemented, the first based on the von Mises yield criterion, i.e. using undrained shear strength, and the second based on the Mohr-Coulomb yield criterion. Both have been extended into the post-yield regime by the addition of a strain softening or hardening modulus, H, which allows the cohesion to change based on the magnitude of the accumulated plastic deviatoric strain invariant. Softening behaviour (H is negative) is illustrated in Fig. 3. To account for the spatial variability of the material properties, random fields have been used and mapped directly onto material points, i.e. each material point has a different value of a parameter governing the material behaviour [9]. Random fields allow the generation of statistically similar (i.e. based on the same input mean and standard deviation) independent realisations, with spatial correlation based on the scale of fluctuation (which can be either isotropic or anisotropic).

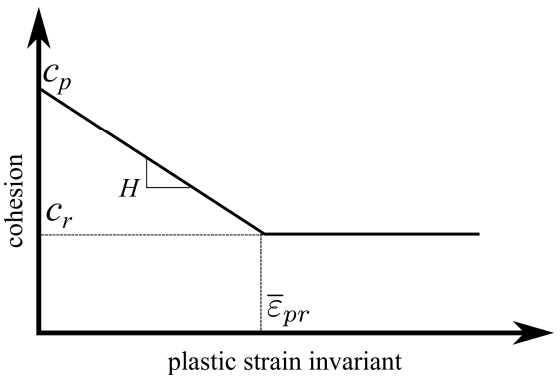

Fig. 3. Schematic of the strain-softening constitutive model [8].

3. Simulations

A case study has been used here, based on a slope with a length significantly greater than the soil depth (see Fig. 4). Hence, a soil depth of 5 m and a horizontal slope length of 26.25 m have been used. A horizontal section of the domain has been included to avoid boundary effects, as has an additional 1:1 (relative to the base of the soil layer) steeper slope at the slope toe, to simulate a triggering situation, e.g. toe erosion or an additional cutting. The lateral boundary conditions are rollers, allowing only vertical displacements, with the base fixed. The ground surface is free and, for hydro-mechanical simulations, the top layer of material points has a fixed value of zero pore pressure. The mesh base and sides are impermeable in hydro-mechanical analyses.

The insitu stresses are generated in a single load step at the start of the analysis and the slope is then allowed to fail. In total stress analyses, all of the slopes are initially unstable. In the hydro-mechanical analyses, an initial suction of 50 kPa is chosen, yielding an initially stable slope. The soil permeability and retention behaviour have been selected such that a sharp saturation font moves (vertically) through the soil, and the failure occurs quickly compared to the rate of saturation.

Three cases are presented below, with the material properties given in Table 1. Two of these case results have been previously presented separately [8,10]. The first case is an undrained (total stress) analysis, with three sub-cases involving different slope angles. The second case is a heterogeneous undrained analysis, with an anisotropic shear strength distribution in which the spatial correlation length in the horizontal direction is 12 times that in the vertical. The third case is a rainfall-induced analysis, which considers a cohesive-frictional soil based on effective stress, and two different residual cohesions.

In all analyses, prior to yield, an elastic behaviour is considered, with a Young's modulus of 1000 kPa and a Poisson's ratio of 0.33. An initial volumetric weight of 20.0 kN/m^3 was considered in Cases 1 and 2, and 22.0 kN/m^3 in Case 3.

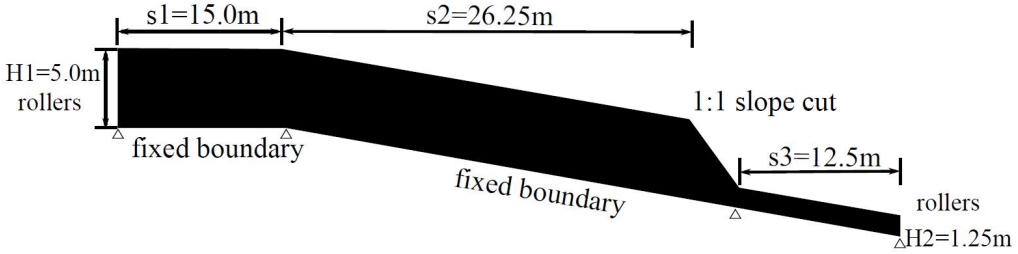

Fig. 4. Numerical case study domain (not to scale).

Table 1. Material properties for the case studies.

Property / Case	1. Undrained / slope angle	2. Heterogeneous	3. Rainfall induced
Total / effective stress analysis	Total	Total	Effective
Slope angles considered (°)	5.0, 10.0, 15.0, 20.0	20.0	20.0
Peak undrained shear strength or effective cohesion, c_p (kPa)	20.0	μ = 20.0 σ = 5.0	20.0
Residual undrained shear strength or effective cohesion, c_r (kPa)	5.0	μ = 5.0 σ = 1.25	0.1, 5.0
Hardening / softening modulus, H (kPa)	-75.0	-50.0	-50.0
Effective friction angle, ϕ (°)	-	-	20

N.B. μ = mean; σ = standard deviation

3.1. Results and discussion

The results for Case 1 are presented in Fig. 5. In Fig. 5(a), the 5° slope fails in a spread form (Fig. 1(f)), where horst and graben type failure blocks can be observed. The failure is triggered by an initial rotational slide at the toe of the slope, and then moves upslope with each of the individual failures occurring separately as lateral support is removed. In Figs. 5(b) and (c), there is also an initial rotational failure at the slope toe, which triggers a translational slide in the slope, with secondary failures occurring as the translational failure develops progressively. In Fig. 5(d) two failures occur simultaneously, a small rotational failure at the toe and a large translational failure (Fig. 1(b)), with the translational failure breaking up as the translation progresses downslope.

The results for Case 2 are shown in Fig. 6. The initial peak cohesion is shown in Fig. 6(a), which is also directly proportional to the residual cohesion. Fig. 6(b) shows that the failure involves multiple failure zones, including one that propagates from the toe and another that propagates from mid-way up the slope. Neither of the major shear bands follows the base of the slope entirely, unlike those shown in Fig. 5, due to the distribution of strong and weak zones in the soil layer. The mechanism includes a series of smaller rotational and translational failures, with rotations mainly being found at the crest and toe of the slope and multiple translational failures occurring in between.

Fig. 7 shows results for pore pressure and plastic strain invariant for Case 3. In Figs. 7(a) and (b), the analysis with a low residual cohesion is shown. After the initial failure is triggered, a series of failures occur, with additional failures being both relatively superficial and occurring in a frictional manner, in an earthflow type landslide (Fig. 1(d)). Eventually, almost all of the slope fails, with almost all of the possible material being incorporated into the landslide. In Figs. 7(c) and (d), the pore pressure and plastic strain invariant are presented for the analysis with a higher residual cohesion. Again, after the initial failure a series of failures are triggered. However, these seem to be rotational (e.g. Fig. 1(e)), with only a relatively small amount of material flowing as an earthflow and the run-out being significantly reduced. A final stepped situation at the upper part of the slope is seen, with an earthflow visible near the toe.

Based on the landslide mechanism classification given in Fig. 1 for geotechnical failures, the majority of failure types can be observed in the numerical analyses undertaken with MPM. It is clear that it is important to characterise the material behaviour, both pre- and post-failure, as it significantly impacts the landslide geometry and final result, e.g. the run-out.

By comparing the analyses presented, a number of aspects are important for consideration in terms of quantification of the hazard. The first is that the initial failure, often characterised in FEM or LEM analyses, is often not representative of the entire failure (Figs. 5 and 6) and variability of material properties contributes extensively to this extended failure. The second is that post-failure constitutive behaviour can govern how the failure develops, e.g. the run-out, and therefore the hazard (Fig. 7).

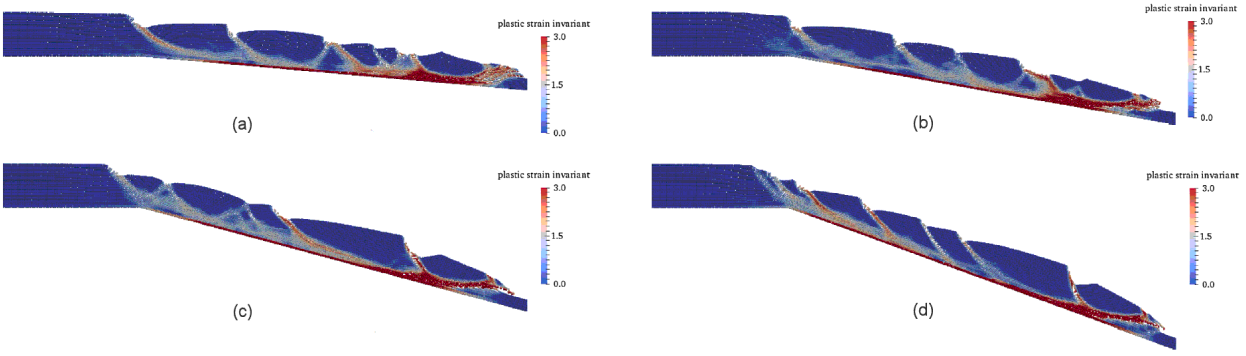

Fig. 5. Results for Case 1: (a) 5° slope; (b) 10° slope; (a) 15° slope; (a) 20° slope.

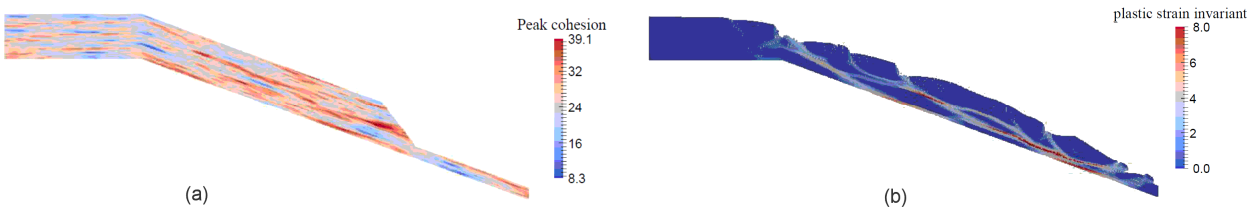

Fig. 6. Results for Case 2: (a) peak cohesion (kPa); (b) plastic strain invariant.

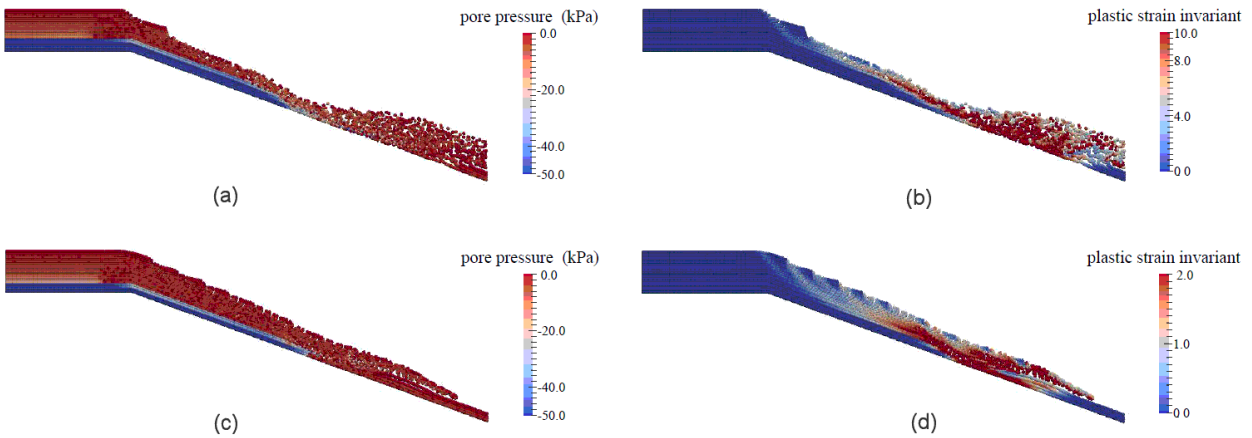

Fig. 7. Results for Case 3: (a) pore pressure with low residual cohesion; (b) plastic strain invariant with low residual cohesion; (c) pore pressure with high residual cohesion; (d) plastic strain invariant with high residual cohesion.

4. Conclusion

This paper presents a summary of an investigation into the computation of slope failures. It also compares observed and simulated mechanisms using the material point method. A series of analyses are reported, illustrating almost the full range of observed failure mechanisms. It is shown that differences in the final geometry can result, influencing the consequence and therefore the risk due to failure. It is also shown to be important to characterise both the pre- and post-failure material behaviour, as both have an influence on the failure mechanism.

References

[1] T. Van Asch, W. Brinkhorst, H. Buist, P. Vessem, The development of landslides by retrogressive failure in varved clays, Zeitschrift fur Geomorphologie NF, 4 (1984) 165–181.
[2] USGS, Landslide types and processes, Fact Sheet 2004-3072, USGS (2004).
[3] D.J. Varnes, Slope movement types and processes, in R.L. Schuster, R.J. Krizek (Eds.), Landslides-Analysis and Control: National Research Council, Washington, D.C., Transportation Research Board, Special Report 176 (1978) 11–33.
[4] A. Locat, S. Leroueil, S. Bernander, D. Demers, H.P. Jostad, L. Ouehb, Progressive failures in eastern Canadian and Scandinavian sensitive clays, Can. Geotech. J., 48 (2011) 1696–1712.
[5] P.J. Vardon, Climatic influence on geotechnical infrastructure: a review, Environ. Geotech. 2(EG3) (2015) 166-174.

[6] D. Sulsky, Z. Chen, H.L. Schreyer, A particle method for history-dependent materials, Comput. Meth. Appl. Mech. Engng. 118 (1994) 179–196.
[7] B. Wang, P.J. Vardon, M.A. Hicks, Z. Chen, Development of an implicit material point method for geotechnical applications, Comput. Geotech. 71 (2016) 159-167.
[8] B. Wang, P.J. Vardon, M.A. Hicks, Investigation of retrogressive and progressive slope failure mechanisms using the material point method, Comput. Geotech. 78 (2016) 88-98.
[9] B. Wang, M.A. Hicks, P.J. Vardon, Slope failure analysis using the random material point method, Géotechnique Letters 6(2) (2016) 113-118.
[10] B. Wang, P.J. Vardon, M.A. Hicks, Preliminary analysis of rainfall-induced slope failures using the material point method, Landslides and Engineered Slopes, Experience, Theory and Practice, Proceedings of the 12th International Symposium on Landslides, Naples (2016) 2037-2042.